

Formation of colour centres in lead-iodide perovskites: Self-trapping and defects in bulk and surfaces

Francesco Ambrosio,^{a,b,*} Edoardo Mosconi,^b Ahmed A. Alasmari,^{c,d} Fatmah A. S. Alasmary,^e Daniele Meggiolaro,^b Filippo De Angelis^{a,b,e,f*}

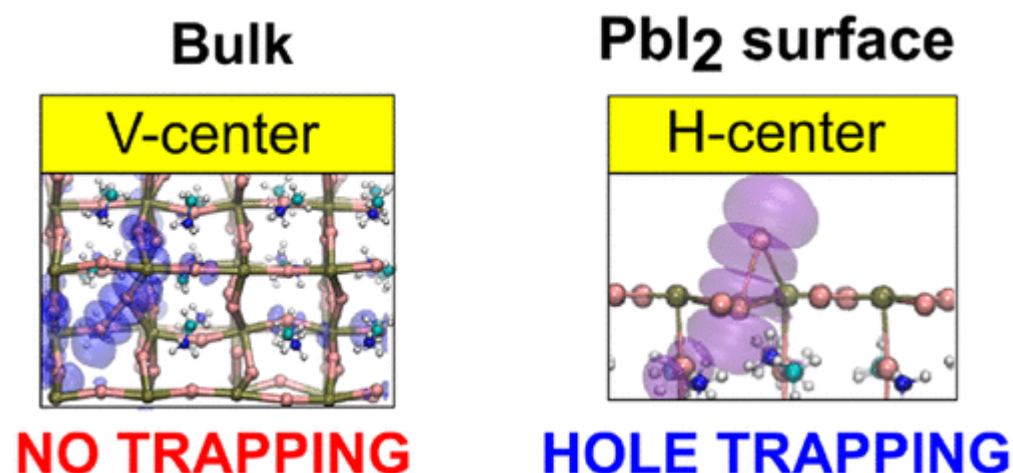
^aCompuNet, Istituto Italiano di Tecnologia, Via Morego 30, 16163 Genova, Italy. ^bComputational Laboratory for Hybrid/Organic Photovoltaics (CLHYO), Istituto CNR di Scienze e Tecnologie Chimiche “Giulio Natta” (CNR-SCITEC), Via Elce di Sotto 8, 06123 Perugia, Italy.

^cThe First Industrial Institute, TVTC, Riyadh, Saudi Arabia. ^dPhysics and Astronomy Department, College of Science, King Saud University, Riyadh, Saudi Arabia.

^eChemistry Department, College of Science, King Saud University, Riyadh, Saudi Arabia. ^fDepartment of Chemistry, Biology and Biotechnology, University of Perugia, Via Elce di Sotto 8, 06123 Perugia, Italy.

*E-mail: Francesco.Ambrosio@iit.it, filippo@thch.unipg.it

Abstract



Self-trapping of excitons or of free charges associated with the formation of color centers is typical of conventional halides. By analogy, lead halide perovskites could in principle show self-trapping of photogenerated charge carriers, possibly leading to defect formation and long-term material instability. Here we investigate the energetics of hole self-trapping in methylammonium lead iodide (MAPbI₃) by performing first-principles electronic structure calculations. The thermodynamics and kinetics for the formation of bridging I₂⁻ dimers and iodine vacancy/I₃⁻ trimer Frenkel defects, originated by self-trapping of one and two holes, respectively, are investigated both in the bulk and at selected surfaces, in both pristine and defective systems. Our results indicate that hole self-trapping is unlikely to occur in the bulk, being thermodynamically unfavorable with associated high-energy barriers. Self-trapping remains unfavorable at surfaces, though it is significantly stabilized compared to the bulk. The inclusion of typical hole-trapping defects, such as the lead vacancy and the interstitial iodine, further stabilizes the formation of color centers, which eventually become stable for the PbI₂-terminated MAPbI₃ surface. Overall, our results clearly indicate that surfaces and grain boundaries are the main instability sources in lead iodide perovskites and that tailoring surface passivation is crucial for improving the performance and long-term stability of devices based on lead halide perovskites.

Introduction

The exceptional optoelectronic properties exhibited by lead halide perovskites (LHPs) have created significant excitement for the immediate potential applications in photovoltaics but have attracted, at the same time, significant interest from a basic science point of view due to their elusive nature.^(1–4) While photoconversion efficiencies of solar cells based on optimized LHP compositions have rapidly exceeded 25%,⁽⁵⁾ achieving a global comprehension of the fundamental physics associated with these excellent performances has proven to be quite challenging for both experimental and theoretical models.^(6,7) In this regard, the fate and dynamics of photogenerated charge carriers remain the main issue to be investigated. In this context, the formation of spatially separated hole and electron polarons in LHPs,^(8,9) due mainly to the distortions in the soft inorganic lattice,^(10–12) has provided hints about some of the outstanding properties of LHPs,^(11–13) such as the slow bimolecular recombination coefficients,^(11–15) the low mobility of charge carriers,⁽¹⁴⁾ and the defect tolerance.^{(15)–(22)} Notwithstanding the recent progress, the description of some features regarding the trapping of photogenerated charge carriers remains controversial. In particular, LHPs belong to the vast family of halides for which the appearance of so-called self-trapped excitons (STEs) and the consequent formation of color centers⁽²³⁾ are widely documented, e.g., in alkaline and alkaline-earth halides.^(23–25) This phenomenon, eventually leading to the trapping of electrons and holes on halide vacancies and interstitials, respectively, is traditionally described as being initiated by the formation of a metal (M)-bridging X_2^- dimer upon trapping of a photogenerated hole.⁽²⁶⁾ This defect, called a V center, involves the interaction and the displacement from their lattice sites of a neutralized halide and a X^- .⁽²⁶⁾ Analogously, the interaction of an interstitial and a lattice halide leads to the formation of a so-called H center.⁽²⁵⁾ It is therefore tempting to explain some of the electronic properties of LHPs by invoking the occurrence of STEs, in analogy with other halides.⁽²⁷⁾ In particular, the formation of STEs localized on I_2^- dimers in MAPbI₃ (MA = methylammonium) has been proposed by electronic structure calculations.^(28,29) It was suggested that the measured high diffusion length of holes in MAPbI₃ could be associated with such self-trapped holes, on the basis of shallow trapping and of the low-energy barriers estimated for the hopping of the defect.⁽²⁸⁾ The formation of Pb-bridging I_2^- dimers was also proposed as an active mechanism of charge trapping in CsPbI₃.⁽²⁷⁾ A possibly related self-trapping phenomenon was further proposed, which involved the formation of an iodine Frenkel defect (IFD), i.e., formation of an interstitial/vacancy I_i^+/V_i^+ couple, under hole-rich conditions.⁽³⁰⁾ The proposed mechanism involves the displacement of a lattice iodine from its position and the simultaneous formation of positively charged I vacancy and I interstitial, upon trapping of two holes.⁽³⁰⁾ Despite being thermodynamically feasible, this mechanism requires a very high concentration of holes,⁽³⁰⁾ although it is worth being considered as it may represent a perovskite degradation pathway. Moreover, the observed photoinduced degradation of MAPbI₃ has recently been explained in terms of a bimolecular reaction that involves the formation of I₂ from Pb-bridging I_2^- dimers and has been found to be viable only at a high concentration of I interstitials.^(15,31) While this result suggests that hole-trapping processes in bulk MAPbI₃ are mainly mediated by impurities, the possibility of self-trapping at the surface of MAPbI₃ has not yet been addressed. In this regard, it has been proposed that instability and charge loss in perovskite-based solar cells may be related to surface effects,^(32,33) the surface trap density was actually found to be ≤ 2 orders of magnitude larger than that of the bulk material, and the diffusion length of charge carriers was noticeably shorter.⁽³⁴⁾ Therefore, it is relevant to understand whether charge trapping at the surface of halide perovskites is unavoidable because of self-trapping or if it can be mediated only by defects (cf. refs ⁽³¹⁾ and ⁽³⁵⁾), which, instead, can be reduced and passivated by chemical treatments or hindered through doping and alloying.^(31,36–45)

In this paper, we investigate through advanced electronic structure calculations the possible sources of charge self-trapping in MAPbI₃, both in the bulk and at representative surfaces. We note that self-trapping of one electron at a MAI-vacant MAPbI₃ surfaces was calculated to be moderately unfavorable (by 0.10 eV).⁽³⁵⁾ Similarly, two-electron trapping at iodine vacancies, previously envisaged through the formation of

a Pb_2^{2+} dimer,⁽⁴⁶⁾ was found to be unstable.⁽⁴⁷⁾ On the basis of this background, here we focus on the thermodynamics and kinetics of hole trapping. We find that both the formation of a Pb-bridging I_2^- dimer and that of IDFs are implausible for the bulk phases as they are thermodynamically and kinetically impeded in pristine tetragonal and orthorhombic MAPbI_3 . When considering the MAPbI_3 surface, we notice that the MAI-terminated surface, corresponding to full surface passivation, is even less supportive than the bulk material with respect to the formation of these moieties. In contrast, self-trapped holes are partly stabilized only when occurring at a PbI_2 -terminated surface, representative of a fully unpassivated surface. This suggests that passivation of undercoordinated Pb sites is crucial to prevent possible endogenous degradation pathways. Furthermore, we observe that the inclusion of commonly encountered defects in MAPbI_3 , such as Pb vacancies and I interstitials, aids the stabilization of hole-trapping species and lowers the energy barriers associated with their formation. We verify that MAPbI_3 degradation under hole-rich conditions, commonly associated with the ejection of molecular iodine from the surface, can occur when PbI_2 layers are (partially) exposed to the surface. Therefore, this phenomenon can be avoided by appropriate surface treatment. Our results highlight the key role of surface properties in determining the performance and long-term stability of devices based on lead halide perovskites.

Methods

To provide an accurate representation of the electronic and trapping properties of MAPbI_3 , we resort to high-level calculations at the hybrid functional level of theory. In particular, we carry out hybrid density functional theory (DFT) calculations at the PBE0+rVV10 level of theory.^(48–51) The fraction of Fock exchange α is kept fixed at its original value (0.25), as it has been found to comply with the Koopmans condition⁽⁵²⁾ for MAPbI_3 , thus ensuring that the calculations are not biased by the self-interaction error,⁽¹¹⁾ which would alter the energetics of the system. We include nonlocal van der Waals interactions through the rVV10 scheme, in which the b parameter governing the extent of long-range interactions is set to its original value of 6.3.^(50,51) All calculations are carried out with the freely available CP2K suite of codes.⁽⁵³⁾ Goedecker–Teter–Hutter pseudopotentials are used to account for core–valence interactions.⁽⁵⁴⁾ We use double- ζ polarized basis sets for the wave functions⁽⁵⁵⁾ and a cutoff of 300 Ry for the expansion of the electron density in plane waves. We employ the auxiliary density matrix method to accelerate the calculation of exact exchange in hybrid functional calculations as implemented in CP2K with the cFIT auxiliary basis set.⁽⁵⁶⁾ Spin-polarized calculations are performed on systems bearing an odd number of electrons.

We do not include spin–orbit coupling (SOC) in the calculations here reported. While significantly contributing to the electronic properties of lead halide perovskites^(57,58) the effect of SOC on valence band-edge states is rather limited.⁽⁴⁷⁾ This ensures that the properties of hole polarons, which originate from the valence band, are properly captured by our computational approach. Nevertheless, the effects of SOC on the energetics of hole-trapping species in the orthorhombic phase of MAPbI_3 have been investigated and found to be exiguous (cf. the [Supporting Information](#) for details of the calculations and of the models employed), in accord with previous studies.^(47,59)

Calculations of energy barriers are carried out using a modified version of the linear transit method⁽⁶⁰⁾ previously employed in ref ⁽¹²⁾. The coordinates of the structures, R_i and R_j , are linearly interpolated⁽⁶⁰⁾ according to the expression $R_\lambda = \lambda R_i + (1 - \lambda)R_j$, where λ is the coupling parameter connecting the two models. The initial and final models (R_i and R_j , respectively) are obtained by relaxing both MA cations and the inorganic lattice. For the R_λ structures obtained by linear interpolation of coordinates R_i and R_j , we follow a procedure ideated and tested in ref ⁽¹²⁾ to calculate energy barriers from structural configurations achieved from molecular dynamics simulations at room temperature. Because the linear interpolation of the coordinates of freely rotating cations can yield highly energetic structures, the R_λ coordinates of MA cations are relaxed while keeping fixed the intermediate R_λ coordinates of the inorganic lattice, instead of just relaxing the wave function, as in the standard linear transit method. We

note that in the case of 0 K calculations, like those performed herein, the displacement of MA cations between reactants and products is exiguous, and therefore, the unmodified linear transit method is actually sufficient to produce accurate results. Indeed, by relaxing MA cations in R_λ , we achieve energy differences of <0.01 eV with respect to the unrelaxed R_λ systems.

Results and Discussion

We first consider the introduction of a single hole in tetragonal MAPbI₃. To sample the possible hole localization induced by thermal disorder, we analyze the first peak of the I–I radial distribution function [$g_{II}(r)$] obtained by 8 ps hybrid-DFT molecular dynamics simulations performed in the presence on an extra hole (cf. [Figure 1a](#)).^(11,12) A majority of the recorded I–I distances are not compatible with the formation of the I₂[−] dimer, whose equilibrium length is 3.3 Å. The small tail in $g_{II}(r)$ appearing below 3.5 Å represents a few of the shorter distances that occur during the MD simulation. By analyzing the I–I distances for each sampled configuration, we find that I–I distances of ≤3.5 Å represent ~5% of the total configurations sampled during the MD and correspond to two lattice iodines bound to the same Pb moving closer together. We then analyze the hole localization for the structural configuration in which the shortest I–I distance is recorded throughout the entire simulation. The hole is found as a polaron on a PbI₂ plane (cf. [Figure 1b](#)), in line with what is observed during the molecular dynamics,^(11,12) thus indicating that no hole localization on this transiently formed I₂[−] dimer actually takes place.

Figure 1

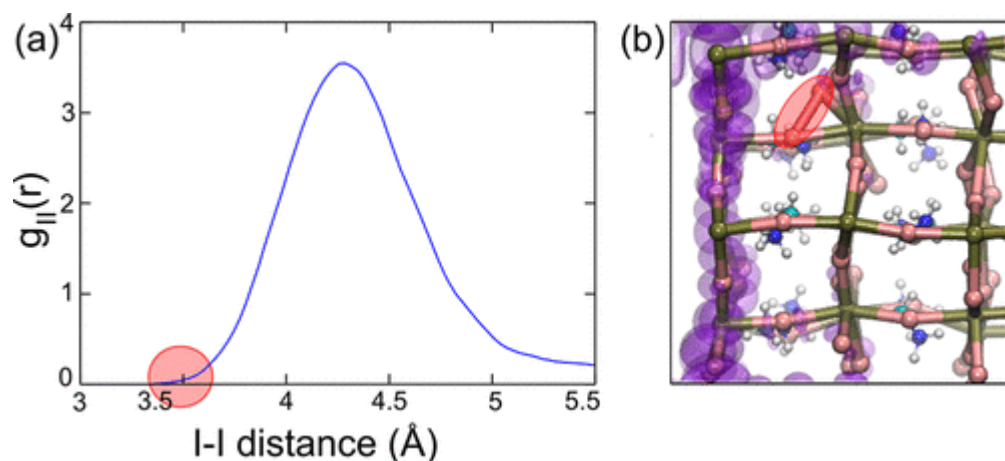
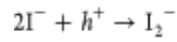


Figure 1. (a) I–I radial distribution function in tetragonal MAPbI₃ as achieved from an 8 ps molecular dynamics simulation of the system with an extra hole. (b) Isodensity representation of the hole wave function for the structural configuration featuring the shortest I–I distance (3.35 Å, highlighted with a red circle). The tetragonal axis lies horizontally.

Because localization of a positive charge with formation of an I₂[−] dimer might involve an energy barrier, this could prevent us from observing this event on a picosecond time scale of *ab initio* molecular dynamics simulations, despite the occurrence of configurations with shortened I–I bonds. For this reason, we performed “static” electronic structure calculations exploring the potential energy surfaces of different models of bulk MAPbI₃ and of related surfaces (cf. the [Supporting Information](#) for the details of the considered models). For each system, we calculate the total energy differences between pristine models with an extra hole and those bearing an I₂[−] dimer (*vide infra*). We first consider the most stable structural model of tetragonal MAPbI₃, corresponding to an ordered arrangement of the MA cations.⁽⁶¹⁾ On this model, we perform two different calculations. (i) We inject an extra hole and relax the structure, and (ii) we move two iodine atoms at a bond length of 3.3 Å to create an I₂[−] dimer (i.e., a V center) and relax the structure with an extra hole. For the former, the hole is found to be delocalized as no hole polaron can be formed in the absence of a localizing field induced by A-site cations.⁽¹²⁾ For the latter, upon relaxation, the

dimer is retained with the hole being localized on it, with the appearance of a Kohn–Sham energy level 0.51 eV above the valence band maximum (VBM) of the material. We then consider the reaction that brings the V center from the capture of an injected hole:



(1)

$$\Delta E(V) = E(\text{I}_2^-) - E(2\text{I}^- + h^+)$$

(2)

where $\Delta E(V)$ is the energy of the supercell bearing a dimer and $E(2\text{I}^- + h^+)$ the energy of the pristine supercell relaxed in the presence of an extra hole. A $\Delta E(V)$ value of 0.50 eV is calculated here (cf. [Figure 2a](#)), thus indicating that dimer formation is strongly disfavored. We then employ a modified version of the linear transit method⁽⁶⁰⁾ (cf. [Methods](#)) to calculate the energy barrier associated with the formation of the Pb-bridging I_2^- . The calculation evidences an energy barrier of 0.60 eV (cf. [Figure 2a](#)) to reach the dimer structure from the starting configuration in which the hole is semilocalized, consistent with the endothermic nature of this process. Then, we consider the orthorhombic phase of MAPbI_3 (o- MAPbI_3) for which previously self-trapping of holes, through formation of an I_2^- dimer, has been suggested.⁽²⁸⁾ A $\Delta E(V)$ value of 0.32 eV is calculated, thus indicating also in this case that hole self-trapping with I_2^- dimer formation is energetically unfavorable. We note that opposite I atoms in o- MAPbI_3 (4.2 Å) are closer than in tetragonal MAPbI_3 (5.6 Å), consistent with the more favorable energetics.

Figure 2

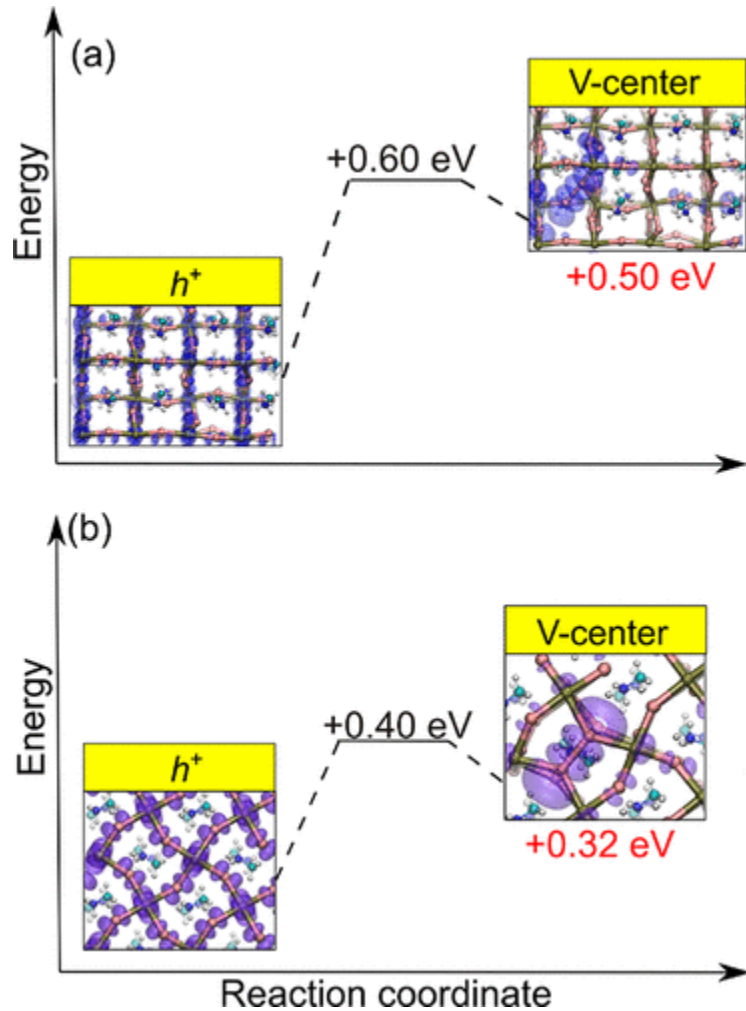
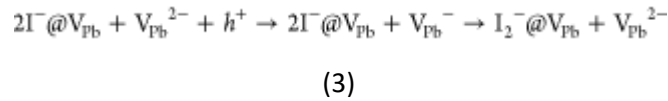


Figure 2. Schematic representation of the energetics associated with trapping of a single hole in (a) tetragonal and (b) orthorhombic MAPbI₃. Pb atoms are colored brown, I atoms pink, C atoms cyan, N atoms blue, and H atoms white. The isodensity representation of the hole is shown in purple shades for each system. The tetragonal axis lies horizontally. A closer representation is given for V centers, to aid their visualization. In each panel, the energies are referred to that of the reactant.

Previous DFT+U calculations indicated that the I₂⁻ dimer in o-MAPbI₃ is energetically favored by as much as 0.19 eV.⁽²⁸⁾ For this reason, we performed additional calculations employing the same computational setup of ref ⁽²⁸⁾ (cf. the [Supporting Information](#)) and verified that only for extreme values of the Hubbard-like term in DFT+U calculations^(62,63) is the dimer energetically favored. In contrast, calculations of $\Delta E(V)$ including relativistic effects and an extended *k*-point sampling confirm the trend here presented (cf. the [Supporting Information](#)). At the highest level of theory employed so far on this system [2 × 1 × 2 orthorhombic supercell – 196 atoms, 1–2–1 *k*-point mesh, hybrid functional + SOC relaxation (cf. the [Supporting Information](#))], we calculate the dimer to be 0.46 eV higher than the pristine bulk, allowing us to safely discard the spontaneous hole self-trapping with formation of an I₂⁻ dimer for both kinetic and thermodynamic reasons.

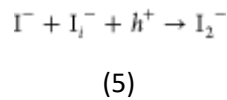
As previously noticed, the presence of defects such as the lead vacancy, V_{Pb}, and the interstitial iodine, I_i, could promote the formation of I₂⁻ dimers in MAPbI₃.^(15,47,64) For hole trapping at V_{Pb}, we consider the following reaction and its energetics:



$$\Delta E(\text{V} @ \text{V}_{\text{Pb}}) = E(\text{I}_2^- @ \text{V}_{\text{Pb}} + \text{V}_{\text{Pb}}^{2-}) - E(2\text{I}^- @ \text{V}_{\text{Pb}} + \text{V}_{\text{Pb}}^-)$$

(4)

Similarly, we can have hole trapping on a I₂⁻ dimer, through the interaction of a lattice iodine with an interstitial I, with the formation of a so-called H center:



$$\Delta E(\text{H}) = E(\text{I}_2^-) - E(\text{I}^- + \text{I}_i^- + h^+)$$

(6)

in which the injected hole is first semilocalized as a hole polaron and then is trapped, thus forming the I₂⁻ moiety.

We thus investigate further the energetics of hole localization at the defect site, searching for favorable energy pathways leading to the lowest barriers and most stable products, being representative of kinetically and thermodynamically preferred pathways, respectively. For hole trapping at V_{Pb}, we calculate the formation of the dimer to occur with either a lower barrier (0.21 eV) leading to a slightly unfavorable energy minimum [$\Delta E(\text{V} @ \text{V}_{\text{Pb}}) = 0.07$ eV] or a higher barrier (0.30 eV) but with a more stable dimer [$\Delta E(\text{V} @ \text{V}_{\text{Pb}}) = -0.12$ eV], as illustrated in panels c and d of [Figure 3](#). Similarly, hole trapping at I_i⁻ may occur with a lower energy barrier (0.10 eV) but leading to a slightly unfavorable minimum [$\Delta E(\text{H}) = 0.05$ eV] or proceed with a slightly higher energy barrier (0.16 eV) but leading to a more stable I₂⁻ dimer [$\Delta E(\text{H}) = -0.14$ eV (cf. [Figure 3](#)c,d)]. The only difference between the two defects is that in I_i⁻ the hole is initially delocalized while a partly localized hole around the lead vacancy is observed (compare structures on the left side of panels a and b of [Figure 3](#) and panels c and d of [Figure 3](#)). Trapping at acceptor defects is thus predicted to

occur through small energy barriers in MAPbI₃, which may contribute to reduce the activity of such defects and enhance the defect tolerance of lead iodide perovskites.[\(13\)](#)

Figure 3

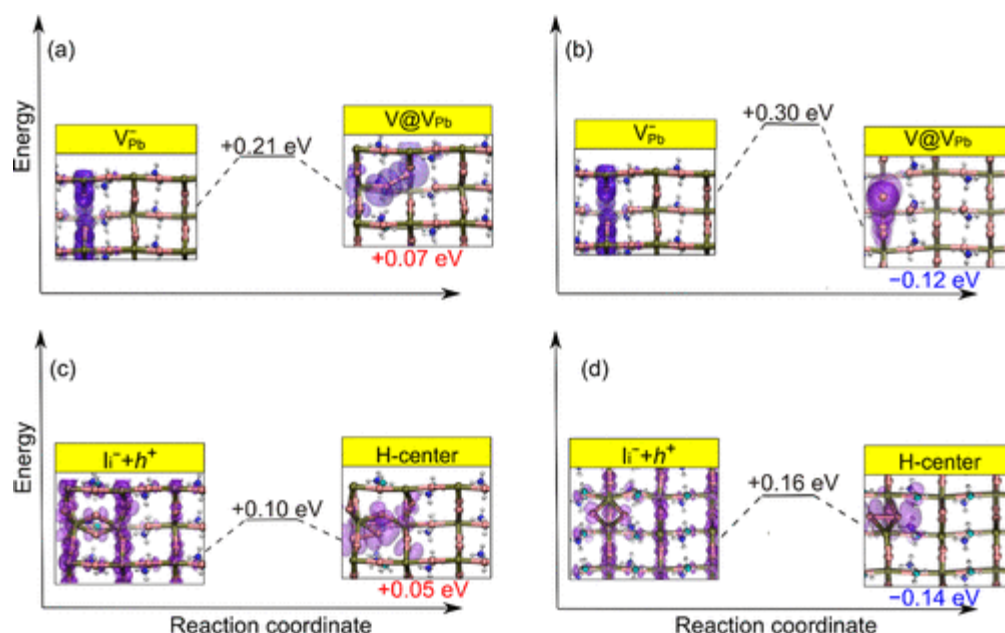


Figure 3. Schematic representation of the energetics associated with trapping of a single hole in a model of tetragonal MAPbI₃ bearing a Pb vacancy and an I interstitial. (a and c) Reaction pathways associated with the lowest energy barriers and (b and d) reaction pathways giving the most stable products. Pb atoms are colored brown, I atoms pink, C atoms cyan, N atoms blue, and H atoms white. The isodensity representation of the hole is colored purple for each system. The tetragonal axis lies horizontally. In each panel, the energies are referred to that of the reactant.

Considering the anticipated impact of surfaces on electron/hole localization and trapping,[\(35,65\)](#) we move to the study of I₂⁻ dimers on the MAPbI₃ surface. We consider the (001) surface of tetragonal MAPbI₃, with two surface terminations, i.e., MAI-terminated and PbI₂-terminated (cf. the [Supporting Information](#) for the details and models), which are representative of a fully passivated and unpassivated surface, respectively. Injection of an extra hole results in the formation of a bulk-like and a surface-localized polaron for the MAI- and PbI₂-terminated surfaces, respectively.[\(35\)](#) For the MAI-terminated surface, a dimer can be achieved only by constraining the I–I distance during geometry optimization. Notably, we do not observe hole trapping on this constrained structure (cf. [Figure 4a](#)), and the unstable dimer structure (0.70 eV above the delocalized hole) immediately breaks if the constraint on the bond length is removed. This result is in line with the lower work function of the MAI perovskite termination impeding charge localization at states above the high-lying valence band.[\(66,67\)](#) Localization of the positive charge on a Pb-bridging I₂⁻ dimer in the pristine PbI₂-terminated slab is instead only slightly energetically disfavored [$\Delta E(V) = 0.07$ eV (cf. [Figure 4b](#))], although this process still features an appreciably high energy barrier (0.31 eV). These results highlight that unsaturated surface Pb atoms may play a major role in favoring charge trapping.

Figure 4

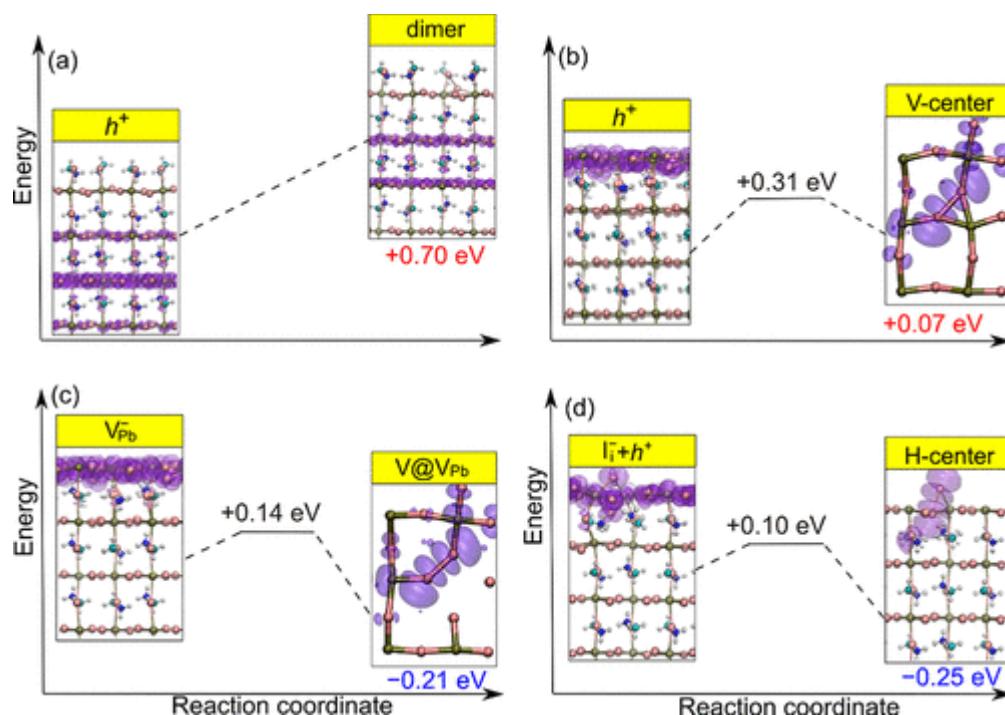


Figure 4. Schematic representation of the energetics associated with trapping of a single hole on the pristine (a) MAI-terminated and (b) PbI₂-terminated (001) MAPbI₃ surface and on the PbI₂-terminated system with a surface (c) a Pb vacancy and (d) an I interstitial. Pb atoms are colored brown, I atoms pink, C atoms cyan, N atoms blue, and H atoms white. The isodensity representation of the hole is colored purple for each system. A side view with the z axis of the slab lying vertically is represented in the all of the figures, with the exception of V centers in the PbI₂-terminated slabs, for which a top view only showing Pb and I atoms is presented, to aid the visualization of the dimer. In each panel, the energies are referred to that of the reactant.

We then consider hole trapping on V_{Pb} and I_i on the PbI₂-terminated slab, because these defects have been found to be particularly stable on this surface termination.^[35] The I₂⁻ dimer is significantly stabilized in both cases with a $\Delta E(V@V_{Pb})$ of -0.21 eV and a $\Delta E(H)$ of -0.25 eV, respectively. We note that the injected hole is drawn to the terminal PbI₂ layer bearing the defect as a surface polaron for both V_{Pb} and I_i (cf. Figure 5a,b). This, in conjunction with the low energy barriers calculated [0.14 and 0.10 eV for hole trapping at V_{Pb} and I_i, respectively (cf. Figure 4)], implies a high probability of reaction and therefore of charge trapping at these surface defects. Considering the high defect density at surfaces and grain boundaries, this highlights how surface passivation is a major strategy to be pursued to further improve nonradiative deactivation of photogenerated charge carriers.

Figure 5

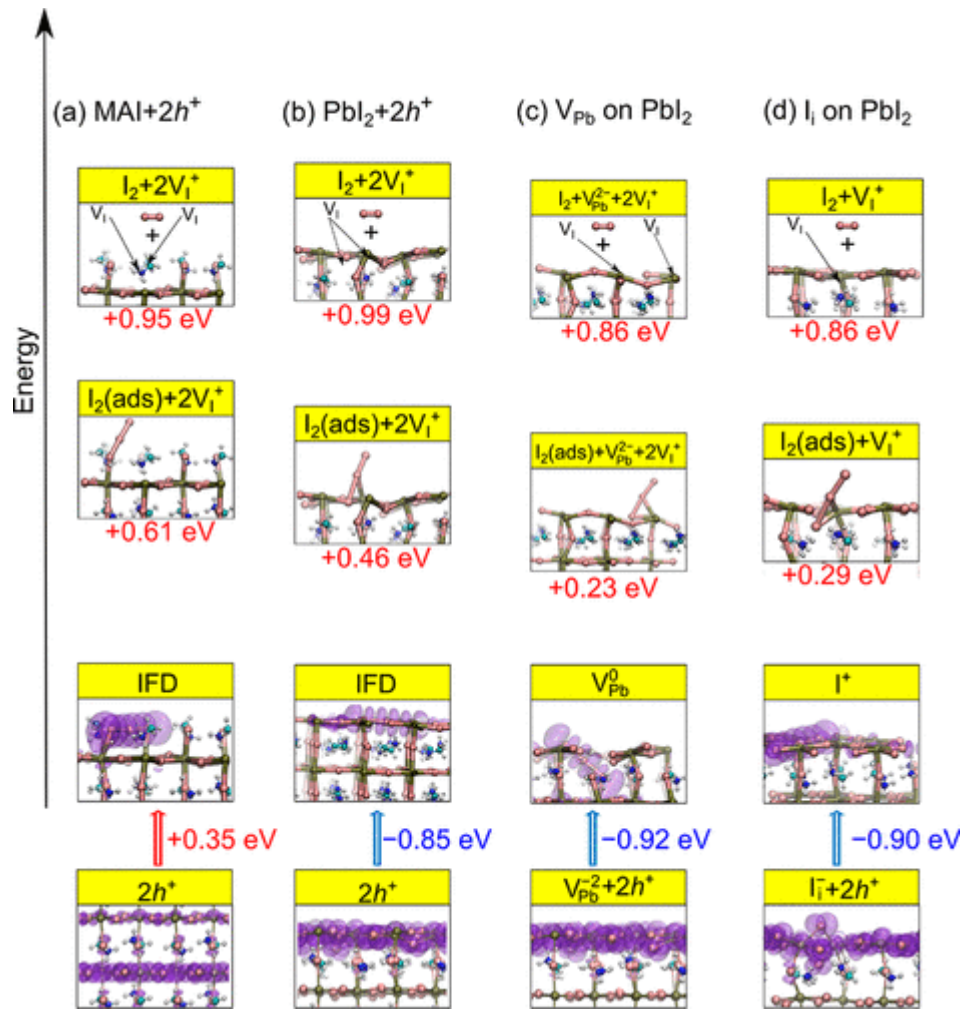
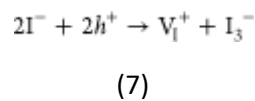


Figure 5. Schematic representation of the energetics associated with trapping of two holes in different models (pristine and defective) of the (001) surface of tetragonal MAPbI₃. For each panel, the energy is that of the structure bearing the IFD/I₃⁻ moiety. For each system, we also include the energy gain/loss associated with hole trapping on the IFD/I₃⁻ moiety. Pb atoms are colored brown, I atoms pink, C atoms cyan, N atoms blue, and H atoms white. The isodensity representation of the hole is colored purple for each system. A side view with the z axis of the slab lying vertically is represented in the all of the figures. The position of surface iodine vacancies is indicated by black arrows.

We next ask what could happen by self-trapping or defect trapping of two charge holes. Despite being kinetically very unlikely, requiring the concomitant trapping of two holes at the same site, this process may become relevant under extremely hole-rich conditions. Kim et al. recently modeled the formation of an iodine vacancy/I₃⁻ trimer Frenkel defect (i.e., an IFD) by the capture of two holes by the perovskite, through the following reaction:

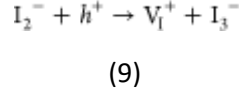


thus involving displacement of a lattice iodide (V_I⁺) and the formation of an I₃⁻ trimer (I₃⁻).⁽³⁰⁾ We thus investigate the energetics of IFD formation in the MAPbI₃ bulk and at surfaces.

We define

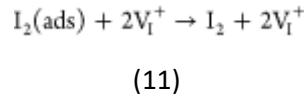
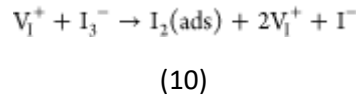
$$\Delta E(\text{IFD}) = E(V_i^+ + I_3^-) - E(2I^- + 2h^+) = E(\text{IFD}) - E(2h^+ + 2I^-) \quad (8)$$

where $E(\text{IFD})$ is the total energy of the supercell with the IFD and $E(2h^+ + 2I^-)$ the total energy of the pristine supercell with two extra holes. We note that



is found to be barrierless for both pristine and defective systems. Therefore, the energy barrier associated with the formation of an IFD is that of the capture of the first hole on the V or H center. For bulk tetragonal MAPbI₃, we calculate a $\Delta E(\text{IFD})$ of 0.24 eV (cf. the [Supporting Information](#)). Therefore, the formation of an IFD is also energetically unfavorable in the pristine bulk perovskite, in line with the results of ref [\(30\)](#). IFD formation is slightly destabilized on the MAI-terminated surface [$\Delta E(\text{IFD}) = 0.35$ eV], for which the trimer is formed on the terminal MAI plane by displacement of an unsaturated I atom (cf. [Figure 5a](#)). This result is in agreement with the observed decreased stability of iodine defects on this termination.[\(35\)](#) In stark contrast, a $\Delta E(\text{IFD})$ of -0.85 eV is calculated for the PbI₂-terminated surface (cf. [Figure 5b](#)), a result consistent with the instability of this surface associated with the lower formation energies calculated for iodine defects on the terminal PbI₂ layer.[\(35\)](#) Therefore, a high concentration of holes can indeed favor the formation of IFDs on the pristine PbI₂-terminated surface. Notably, IFD formation can also favorably occur when a partial MAI coverage leaves the subsurface PbI₂ plane exposed. For instance, when a 50% MAI-covered slab is considered, we find a $\Delta E(\text{IFD})$ of -0.18 eV (cf. the [Supporting Information](#)). IFD formation is favored also at defect sites on the PbI₂-terminated surface, with a stabilization comparable to that in the case of self-trapping (cf. [Figure 5c,d](#)).

Finally, we investigate the possible degradation mechanisms mediated by IFD formation at the MAPbI₃ surface under extremely hole-rich conditions. Starting from the IFD, we consider the following reaction sequence:



which ultimately leads to the loss of molecular iodine from the surface of the pristine material. Similar reactions hold when the process is mediated by a V_{Pb} and I_i . In fact, the I_3^- trimer is found as the most stable forms of V_{Pb}^0 and I_i^+ with energy levels deep in the gap of the material.[\(20,35\)](#)

We calculate the total energies for each step of the reaction for both pristine surfaces and, in the PbI₂-terminated case, in the presence of V_{Pb} and I_i . We find that [reactions 10](#) and [11](#) have comparable energetics once the IFD, or equivalently the I_3^- trimer, has been formed, with I_2 release being ~0.9 eV higher than the corresponding IFD/ I_3^- for all of the considered pristine and defective models (cf. [Figure 5](#)). The reversal of [reaction 11](#), i.e., I_2 adsorption, is favored by 0.4–0.5 eV, in agreement with previous results.[\(68\)](#) The actual energetics of I_2 release is thus connected with the energy required for the formation of the IFD, which in turn is modulated by the surface work function[\(66\)](#) and, therefore, depends on the surface termination. As one may notice, IFD (or again I_3^- trimer) formation on PbI₂-terminated surfaces is favored by ~0.9 eV for both pristine and defective slabs, thus balancing the unfavorable energetics due to I_2 release. We note that this energetics is essentially unaffected by the thickness of the employed slab

model (cf. the [Supporting Information](#)). Furthermore, we note that for I_2 release as a gas-phase molecule, we have to consider an extra stabilization of ~ 0.7 eV in [reaction 11](#), corresponding to the thermal corrections to entropy and enthalpy of gaseous I_2 .[\(68\)](#) Thus, while a high level of hole accumulation does not lead to perovskite degradation for MAI-terminated surfaces, the (partial) exposure of PbI_2 -terminated surfaces under extremely hole-rich conditions may lead to significant degradation of $MAPbI_3$ with release of gas-phase or solvated I_2 .[\(31,69,70\)](#)

Overall, our analysis reveals that self-trapping of holes is undisputedly unfavorable in the bulk material, for both the tetragonal and the orthorhombic phases. In contrast, hole trapping at I_2^- dimers may be promoted by defects such as Pb vacancies and I interstitials, although for the latter a reduced hole capture probability, due to the fast hopping of the hole polaron within the material, could limit its trapping activity.[\(11,12\)](#) This leaves the Pb vacancy as the main possible promoter of hole trapping in the bulk material, because the charge hole tends to be localized on the plane bearing the defect, thus implying a larger probability of hole–defect interaction. The dimer can form more easily on both the pristine and Pb-vacant PbI_2 -terminated surface of $MAPbI_3$. The physical picture is almost equivalent when considering IFDs, whose formation is favored only on the PbI_2 -terminated surface of $MAPbI_3$. Therefore, our results indicate that hole trapping and the possibly related degradation phenomena in $MAPbI_3$ are generally defect-mediated phenomena; however, PbI_2 surfaces can actually induce self-trapping of holes with the formation of IFDs even when pristine. We note, however, that photoinduced degradation can indeed occur when a very high density of defects is considered.[\(31\)](#) In this context, surface treatments on $MAPbI_3$ have a double beneficial effect when saturating undercoordinated sites. (i) They decrease the concentration of charge traps, and (ii) they prevent surface degradation through dissociation of surface-adsorbed I_2 molecules. The reduced charge recombination measured for polycrystalline samples with excess MA cations[\(36\)](#) is consistent with the present physical picture, because MA cations passivate surface defects and unsaturated surface Pb atoms, which are ultimately responsible for charge trapping and photoinduced degradation. We note that such treatments prevent also charge trapping under electron-rich conditions. In fact, unsaturated subsurface lead atoms in MAI-vacant surfaces may actually be detached from the surface as metallic Pb under electron-rich conditions.[\(35,71\)](#) Therefore, it is important to tailor the surface perovskite properties to minimize charge loss and extend the durability of perovskite-based devices.

Conclusions

In summary, hole self-trapping in halide perovskites is demonstrated to be highly unfavorable in bulk $MAPbI_3$ on the basis of both thermodynamics and kinetics. Our calculations instead show that self-hole trapping is essentially a surface phenomenon, taking place at unpassivated surfaces under extremely high hole conditions. As such, this severe instability pathway, which could lead to the expulsion of I_2 from the perovskite under hole-rich regimes, can be avoided by appropriate surface treatment. By accurately quantifying the energetics of self- and defect-mediated trapping in the prototypical $MAPbI_3$ perovskite, we highlight the importance of properly addressing surface effects in metal halide perovskites, possibly stimulating additional dedicated experiments and surface passivation strategies.

Supporting Information

The Supporting Information is available free of charge at <https://pubs.acs.org/doi/10.1021/acs.chemmater.0c02005>.

- A detailed description of the models employed, an analysis of the impact of the thickness of the slab on the electronic properties of IFDs, $\Delta E(V)$ for o- $MAPbI_3$ at various levels of theory, list of $\Delta E(IFD)$ values for different systems, representation of hole trapping in bulk tetragonal $MAPbI_3$ and on the 50% MAI-covered (001) surface, and additional references ([PDF](#))

Terms & Conditions

Most electronic Supporting Information files are available without a subscription to ACS Web Editions. Such files may be downloaded by article for research use (if there is a public use license linked to the relevant article, that license may permit other uses). Permission may be obtained from ACS for other uses through requests via the RightsLink permission system: <http://pubs.acs.org/page/copyright/permissions.html>.

Author Information

- **Corresponding Authors**

- **Francesco Ambrosio** - *CompuNet, Istituto Italiano di Tecnologia, Via Morego 30, 16163 Genova, Italy; Computational Laboratory for Hybrid/Organic Photovoltaics (CLHYO), Istituto CNR di Scienze e Tecnologie Chimiche "Giulio Natta" (CNR-SCITEC), Via Elce di Sotto 8, 06123 Perugia, Italy; <http://orcid.org/0000-0002-6388-9586>; Email: Francesco.Ambrosio@iit.it*
- **Filippo De Angelis** - *CompuNet, Istituto Italiano di Tecnologia, Via Morego 30, 16163 Genova, Italy; Computational Laboratory for Hybrid/Organic Photovoltaics (CLHYO), Istituto CNR di Scienze e Tecnologie Chimiche "Giulio Natta" (CNR-SCITEC), Via Elce di Sotto 8, 06123 Perugia, Italy; Chemistry Department, College of Science, King Saud University, Riyadh 12372, Saudi Arabia; Department of Chemistry, Biology and Biotechnology, University of Perugia, Via Elce di Sotto 8, 06123 Perugia, Italy; <http://orcid.org/0000-0003-3833-1975>; Email: filippo@thch.unipg.it*

- **Authors**

- **Edoardo Mosconi** - *Computational Laboratory for Hybrid/Organic Photovoltaics (CLHYO), Istituto CNR di Scienze e Tecnologie Chimiche "Giulio Natta" (CNR-SCITEC), Via Elce di Sotto 8, 06123 Perugia, Italy; <http://orcid.org/0000-0001-5075-6664>*
- **Ahmed A. Alasmari** - *The First Industrial Institute, TVTC, Riyadh 12613, Saudi Arabia; Physics and Astronomy Department, College of Science, King Saud University, Riyadh 12372, Saudi Arabia*
- **Fatmah A. S. Alasmay** - *Chemistry Department, College of Science, King Saud University, Riyadh 12372, Saudi Arabia*
- **Daniele Meggiolaro** - *Computational Laboratory for Hybrid/Organic Photovoltaics (CLHYO), Istituto CNR di Scienze e Tecnologie Chimiche "Giulio Natta" (CNR-SCITEC), Via Elce di Sotto 8, 06123 Perugia, Italy; <http://orcid.org/0000-0001-9717-133X>*

- **Notes**

The authors declare no competing financial interest.

Acknowledgments

This work was supported by the Distinguished Scientist Fellowship Program (DSFP) of King Saud University. E.M. has received funding from the European Union's Horizon 2020 research and innovation programme under Grant Agreement 764047 of the ESPRESSO project. The Ministero dell'Istruzione dell'Università e della Ricerca (MIUR) and Università degli Studi di Perugia are acknowledged for financial support through the program "Dipartimenti di Eccellenza 2018-2022" (Grant AMIS) to F.D.A.

References

This article references 71 other publications.

1. Etgar, L.; Gao, P.; Xue, Z.; Peng, Q.; Chandiran, A. K.; Liu, B.; Nazeeruddin, M. K.; Grätzel, M. Mesoscopic $\text{CH}_3\text{NH}_3\text{PbI}_3/\text{TiO}_2$ Heterojunction Solar Cells. *J. Am. Chem. Soc.* **2012**, *134* (42), 17396–17399, DOI: 10.1021/ja307789s
2. Burschka, J.; Pellet, N.; Moon, S.-J.; Humphry-Baker, R.; Gao, P.; Nazeeruddin, M. K.; Grätzel, M. Sequential Deposition as a Route to High-Performance Perovskite-Sensitized Solar Cells. *Nature* **2013**, *499*, 316, DOI: 10.1038/nature12340
3. Brenner, T. M.; Egger, D. A.; Kronik, L.; Hodes, G.; Cahen, D. Hybrid Organic—Inorganic Perovskites: Low-Cost Semiconductors with Intriguing Charge-Transport Properties. *Nat. Rev. Mater.* **2016**, *1*, 15007, DOI: 10.1038/natrevmats.2015.7
4. Meggiolaro, D.; Ambrosio, F.; Mosconi, E.; Mahata, A.; De Angelis, F. Polarons in Metal Halide Perovskites. *Adv. Energy Mater.* **2020**, *10*, 1902748, DOI: 10.1002/aenm.201902748
5. National Renewable Energy Laboratory (NREL) website. <https://www.nrel.gov/pv/assets/images/efficiency-chart.png> (accessed 2019-09-13).
6. Filippetti, A.; Delugas, P.; Mattoni, A. Radiative Recombination and Photoconversion of Methylammonium Lead Iodide Perovskite by First Principles: Properties of an Inorganic Semiconductor within a Hybrid Body. *J. Phys. Chem. C* **2014**, *118* (43), 24843–24853, DOI: 10.1021/jp507430x
7. Sell, D. D.; Casey, H. C. Optical Absorption and Photoluminescence Studies of Thin GaAs Layers in $\text{GaAs-Al}_x\text{Ga}_{1-x}\text{As}$ Double Heterostructures. *J. Appl. Phys.* **1974**, *45* (2), 800–807, DOI: 10.1063/1.1663321
8. Miyata, K.; Meggiolaro, D.; Trinh, M. T.; Joshi, P. P.; Mosconi, E.; Jones, S. C.; De Angelis, F.; Zhu, X. Y. Large Polarons in Lead Halide Perovskites. *Sci. Adv.* **2017**, *3* (8), e1701217 DOI: 10.1126/sciadv.1701217
9. Cinquanta, E.; Meggiolaro, D.; Motti, S. G.; Gandini, M.; Alcocer, M. J. P.; Akkerman, Q. A.; Vozzi, C.; Manna, L.; De Angelis, F.; Petrozza, A.; Stagira, S. Ultrafast THz Probe of Photoinduced Polarons in Lead-Halide Perovskites. *Phys. Rev. Lett.* **2019**, *122* (16), 166601, DOI: 10.1103/PhysRevLett.122.166601
10. Yaffe, O.; Guo, Y.; Tan, L. Z.; Egger, D. A.; Hull, T.; Stoumpos, C. C.; Zheng, F.; Heinz, T. F.; Kronik, L.; Kanatzidis, M. G.; Owen, J. S.; Rappe, A. M.; Pimenta, M. A.; Brus, L. E. Local Polar Fluctuations in Lead Halide Perovskite Crystals. *Phys. Rev. Lett.* **2017**, *118* (13), 136001, DOI: 10.1103/PhysRevLett.118.136001
11. Ambrosio, F.; Wiktor, J.; De Angelis, F.; Pasquarello, A. Origin of Low Electron–Hole Recombination Rate in Metal Halide Perovskites. *Energy Environ. Sci.* **2018**, *11* (1), 101–105, DOI: 10.1039/C7EE01981E
12. Ambrosio, F.; Meggiolaro, D.; Mosconi, E.; De Angelis, F. Charge Localization, Stabilization, and Hopping in Lead Halide Perovskites: Competition between Polaron Stabilization and Cation Disorder. *ACS Energy Lett.* **2019**, *4* (8), 2013–2020, DOI: 10.1021/acsenenergylett.9b01353

13. Wiktor, J.; Ambrosio, F.; Pasquarello, A. Mechanism Suppressing Charge Recombination at Iodine Defects in $\text{CH}_3\text{NH}_3\text{PbI}_3$ by Polaron Formation. *J. Mater. Chem. A* **2018**, *6* (35), 16863– 16867, DOI: 10.1039/C8TA06466K
14. Brenner, T. M.; Egger, D. A.; Rappe, A. M.; Kronik, L.; Hodes, G.; Cahen, D. Are Mobilities in Hybrid Organic–Inorganic Halide Perovskites Actually “High”? *J. Phys. Chem. Lett.* **2015**, *6* (23), 4754– 4757, DOI: 10.1021/acs.jpcllett.5b02390
15. Motti, S. G.; Meggiolaro, D.; Martani, S.; Sorrentino, R.; Barker, A. J.; De Angelis, F.; Petrozza, A. Defect Activity in Metal–Halide Perovskites. *Adv. Mater.* **2019**, *31*, 1901183, DOI: 10.1002/adma.201901183
16. Kim, J.; Lee, S.-H.; Lee, J. H.; Hong, K.-H. The Role of Intrinsic Defects in Methylammonium Lead Iodide Perovskite. *J. Phys. Chem. Lett.* **2014**, *5* (8), 1312– 1317, DOI: 10.1021/jz500370k
17. Yamada, Y.; Endo, M.; Wakamiya, A.; Kanemitsu, Y. Spontaneous Defect Annihilation in $\text{CH}_3\text{NH}_3\text{PbI}_3$ Thin Films at Room Temperature Revealed by Time-Resolved Photoluminescence Spectroscopy. *J. Phys. Chem. Lett.* **2015**, *6* (3), 482– 486, DOI: 10.1021/jz5026596
18. Buin, A.; Pietsch, P.; Xu, J.; Voznyy, O.; Ip, A. H.; Comin, R.; Sargent, E. H. Materials Processing Routes to Trap-Free Halide Perovskites. *Nano Lett.* **2014**, *14* (11), 6281– 6286, DOI: 10.1021/nl502612m
19. Dagnall, K. A.; Foley, B. J.; Cuthriell, S. A.; Alpert, M. R.; Deng, X.; Chen, A. Z.; Sun, Z.; Gupta, M. C.; Xiao, K.; Lee, S.-H.; Ma, Y.-Z.; Choi, J. J. Relationship between the Nature of Monovalent Cations and Charge Recombination in Metal Halide Perovskites. *ACS Appl. Energy Mater.* **2020**, *3*, 1298, DOI: 10.1021/acsaem.9b02310
20. Meggiolaro, D.; Motti, S. G.; Mosconi, E.; Barker, A. J.; Ball, J.; Andrea Riccardo Perini, C.; Deschler, F.; Petrozza, A.; De Angelis, F. Iodine Chemistry Determines the Defect Tolerance of Lead-Halide Perovskites. *Energy Environ. Sci.* **2018**, *11* (3), 702– 713, DOI: 10.1039/C8EE00124C
21. Chu, W.; Zheng, Q.; Prezhdov, O. V.; Zhao, J.; Saidi, W. A. Low-Frequency Lattice Phonons in Halide Perovskites Explain High Defect Tolerance Toward Electron-Hole Recombination. *Sci. Adv.* **2020**, *6* (7), eaaw7453, DOI: 10.1126/sciadv.aaw7453
22. Chu, W.; Saidi, W. A.; Zhao, J.; Prezhdov, O. V. Soft Lattice and Defect Covalency Rationalize Tolerance of $\beta\text{-CsPbI}_3$ Perovskite Solar Cells to Native Defects. *Angew. Chem., Int. Ed.* **2020**, *59* (16), 6435– 6441, DOI: 10.1002/anie.201915702
23. Stoneham, A. M. *Theory of defects in solids: electronic structure of defects in insulators and semiconductors*; Clarendon Press: Oxford, U.K., 2001.
24. Sonder, E.; Sibley, W. A. *Point defects in solids*; Plenum Press: New York, 1972.
25. Williams, R. T.; Song, K. S. The Self-Trapped Exciton. *J. Phys. Chem. Solids* **1990**, *51* (7), 679– 716, DOI: 10.1016/0022-3697(90)90144-5
26. Popov, A. I.; Kotomin, E. A.; Maier, J. Analysis of Self-Trapped Hole Mobility in Alkali Halides and Metal Halides. *Solid State Ionics* **2017**, *302*, 3– 6, DOI: 10.1016/j.ssi.2016.12.004
27. Evarestov, R. A.; Senocrate, A.; Kotomin, E. A.; Maier, J. First-Principles Calculations of Iodine-Related Point Defects in CsPbI_3 . *Phys. Chem. Chem. Phys.* **2019**, *21* (15), 7841– 7846, DOI: 10.1039/C9CP00414A

28. Peng, C.; Wang, J.; Wang, H.; Hu, P. Unique Trapped Dimer State of the Photogenerated Hole in Hybrid Orthorhombic $\text{CH}_3\text{NH}_3\text{PbI}_3$ Perovskite: Identification, Origin, and Implications. *Nano Lett.* **2017**, *17* (12), 7724–7730, DOI: 10.1021/acs.nanolett.7b03885
29. Whalley, L. D.; Crespo-Otero, R.; Walsh, A. H-Center and V-Center Defects in Hybrid Halide Perovskites. *ACS Energy Lett.* **2017**, *2* (12), 2713–2714, DOI: 10.1021/acsenergylett.7b00995
30. Kim, S. H.; Lee, D. Role of Charge-Trapping Iodine Frenkel Defects for Hysteresis in Organic–Inorganic Hybrid Perovskite from First-Principles Calculations. *J. Phys. Chem. C* **2019**, *123* (14), 9629–9633, DOI: 10.1021/acs.jpcc.9b01770
31. Motti, S. G.; Meggiolaro, D.; Barker, A. J.; Mosconi, E.; Perini, C. A. R.; Ball, J. M.; Gandini, M.; Kim, M.; De Angelis, F.; Petrozza, A. Controlling Competing Photochemical Reactions Stabilizes Perovskite Solar Cells. *Nat. Photonics* **2019**, *13* (8), 532–539, DOI: 10.1038/s41566-019-0435-1
32. Schulz, P.; Cahen, D.; Kahn, A. Halide Perovskites: Is It All about the Interfaces?. *Chem. Rev.* **2019**, *119* (5), 3349–3417, DOI: 10.1021/acs.chemrev.8b00558
33. Ono, L. K.; Qi, Y. Surface and Interface Aspects of Organometal Halide Perovskite Materials and Solar Cells. *J. Phys. Chem. Lett.* **2016**, *7* (22), 4764–4794, DOI: 10.1021/acs.jpclett.6b01951
34. Wu, B.; Nguyen, H. T.; Ku, Z.; Han, G.; Giovanni, D.; Mathews, N.; Fan, H. J.; Sum, T. C. Discerning the Surface and Bulk Recombination Kinetics of Organic–Inorganic Halide Perovskite Single Crystals. *Adv. Energy Mater.* **2016**, *6* (14), 1600551, DOI: 10.1002/aenm.201600551
35. Ambrosio, F.; Meggiolaro, D.; Mosconi, E.; De Angelis, F. Charge Localization and Tapping at Surfaces in Lead-Iodide Perovskites: The Role of Polarons and Defects. *J. Mater. Chem. A* **2020**, *8* (14), 6882–6892, DOI: 10.1039/D0TA00798F
36. Yang, Y.; Yang, M.; Moore, D. T.; Yan, Y.; Miller, E. M.; Zhu, K.; Beard, M. C. Top and Bottom Surfaces Limit Carrier Lifetime in Lead Iodide Perovskite Films. *Nat. Energy* **2017**, *2*, 16207, DOI: 10.1038/nenergy.2016.207
37. Xu, J.; Buin, A.; Ip, A. H.; Li, W.; Voznyy, O.; Comin, R.; Yuan, M.; Jeon, S.; Ning, Z.; McDowell, J. J.; Kanjanaboos, P.; Sun, J.-P.; Lan, X.; Quan, L. N.; Kim, D. H.; Hill, I. G.; Maksymovych, P.; Sargent, E. H. Perovskite–Fullerene Hybrid Materials Suppress Hysteresis in Planar Diodes. *Nat. Commun.* **2015**, *6*, 7081, DOI: 10.1038/ncomms8081
38. Zhang, H.; Wu, Y.; Shen, C.; Li, E.; Yan, C.; Zhang, W.; Tian, H.; Han, L.; Zhu, W.-H. Efficient and Stable Chemical Passivation on Perovskite Surface via Bidentate Anchoring. *Adv. Energy Mater.* **2019**, *9* (13), 1803573, DOI: 10.1002/aenm.201803573
39. Noel, N. K.; Abate, A.; Stranks, S. D.; Parrott, E. S.; Burlakov, V. M.; Goriely, A.; Snaith, H. J. Enhanced Photoluminescence and Solar Cell Performance via Lewis Base Passivation of Organic–Inorganic Lead Halide Perovskites. *ACS Nano* **2014**, *8* (10), 9815–9821, DOI: 10.1021/nn5036476
40. Yang, S.; Dai, J.; Yu, Z.; Shao, Y.; Zhou, Y.; Xiao, X.; Zeng, X. C.; Huang, J. Tailoring Passivation Molecular Structures for Extremely Small Open-Circuit Voltage Loss in Perovskite Solar Cells. *J. Am. Chem. Soc.* **2019**, *141* (14), 5781–5787, DOI: 10.1021/jacs.8b13091
41. Wang, Q.; Mosconi, E.; Wolff, C.; Li, J.; Neher, D.; De Angelis, F.; Suranna, G. P.; Grisorio, R.; Abate, A. Rationalizing the Molecular Design of Hole-Selective Contacts to Improve Charge Extraction in Perovskite Solar Cells. *Adv. Energy Mater.* **2019**, *9* (28), 1900990, DOI: 10.1002/aenm.201900990

42. Ju, D.; Dang, Y.; Zhu, Z.; Liu, H.; Chueh, C.-C.; Li, X.; Wang, L.; Hu, X.; Jen, A. K. Y.; Tao, X. Tunable Band Gap and Long Carrier Recombination Lifetime of Stable Mixed $\text{CH}_3\text{NH}_3\text{Pb}_x\text{Sn}_{1-x}\text{Br}_3$ Single Crystals. *Chem. Mater.* **2018**, *30* (5), 1556– 1565, DOI: 10.1021/acs.chemmater.7b04565
43. Pisanu, A.; Mahata, A.; Mosconi, E.; Patrini, M.; Quadrelli, P.; Milanese, C.; De Angelis, F.; Malavasi, L. Exploring the Limits of Three-Dimensional Perovskites: The Case of $\text{FAPb}_{1-x}\text{Sn}_x\text{Br}_3$. *ACS Energy Lett.* **2018**, *3* (6), 1353– 1359, DOI: 10.1021/acsenergylett.8b00615
44. Eperon, G. E.; Leijtens, T.; Bush, K. A.; Prasanna, R.; Green, T.; Wang, J. T.-W.; McMeekin, D. P.; Volonakis, G.; Milot, R. L.; May, R.; Palmstrom, A.; Slotcavage, D. J.; Belisle, R. A.; Patel, J. B.; Parrott, E. S.; Sutton, R. J.; Ma, W.; Moghadam, F.; Conings, B.; Babayigit, A.; Boyen, H.-G.; Bent, S.; Giustino, F.; Herz, L. M.; Johnston, M. B.; McGehee, M. D.; Snaith, H. J. Perovskite-Perovskite Tandem Photovoltaics with Optimized Band Gaps. *Science* **2016**, *354* (6314), 861, DOI: 10.1126/science.aaf9717
45. Yang, Z.; Rajagopal, A.; Chueh, C.-C.; Jo, S. B.; Liu, B.; Zhao, T.; Jen, A. K. Y. Stable Low-Bandgap Pb–Sn Binary Perovskites for Tandem Solar Cells. *Adv. Mater.* **2016**, *28* (40), 8990– 8997, DOI: 10.1002/adma.201602696
46. Agiorgousis, M. L.; Sun, Y.-Y.; Zeng, H.; Zhang, S. Strong Covalency-Induced Recombination Centers in Perovskite Solar Cell Material $\text{CH}_3\text{NH}_3\text{PbI}_3$. *J. Am. Chem. Soc.* **2014**, *136* (41), 14570– 14575, DOI: 10.1021/ja5079305
47. Meggiolaro, D.; De Angelis, F. First-Principles Modeling of Defects in Lead Halide Perovskites: Best Practices and Open Issues. *ACS Energy Lett.* **2018**, *3* (9), 2206– 2222, DOI: 10.1021/acsenergylett.8b01212
48. Perdew, J. P.; Ernzerhof, M.; Burke, K. Rationale for Mixing Exact Exchange with Density Functional Approximations. *J. Chem. Phys.* **1996**, *105* (22), 9982– 9985, DOI: 10.1063/1.472933
49. Adamo, C.; Barone, V. Toward Reliable Density Functional Methods without Adjustable Parameters: The PBE0Model. *J. Chem. Phys.* **1999**, *110* (13), 6158– 6170, DOI: 10.1063/1.478522
50. Vydrov, O. A.; Van Voorhis, T. Nonlocal van der Waals Density Functional: The Simpler the Better. *J. Chem. Phys.* **2010**, *133* (24), 244103, DOI: 10.1063/1.3521275
51. Sabatini, R.; Gorni, T.; De Gironcoli, S. Nonlocal van der Waals Density Functional Made Simple and Efficient. *Phys. Rev. B: Condens. Matter Mater. Phys.* **2013**, *87* (4), 041108 DOI: 10.1103/PhysRevB.87.041108
52. Perdew, J. P.; Parr, R. G.; Levy, M.; Balduz, J. L. Density-Functional Theory for Fractional Particle Number: Derivative Discontinuities of the Energy. *Phys. Rev. Lett.* **1982**, *49* (23), 1691– 1694, DOI: 10.1103/PhysRevLett.49.1691
53. VandeVondele, J.; Krack, M.; Mohamed, F.; Parrinello, M.; Chassaing, T.; Hutter, J. Quickstep: Fast and Accurate Density Functional Calculations Using a Mixed Gaussian and Plane Waves Approach. *Comput. Phys. Commun.* **2005**, *167* (2), 103– 128, DOI: 10.1016/j.cpc.2004.12.014
54. Goedecker, S.; Teter, M.; Hutter, J. Separable Dual-Space Gaussian Pseudopotentials. *Phys. Rev. B: Condens. Matter Mater. Phys.* **1996**, *54* (3), 1703, DOI: 10.1103/PhysRevB.54.1703
55. VandeVondele, J.; Hutter, J. Gaussian Basis Sets for Accurate Calculations on Molecular Systems in Gas and Condensed Phases. *J. Chem. Phys.* **2007**, *127* (11), 114105, DOI: 10.1063/1.2770708

56. Guidon, M.; Hutter, J.; VandeVondele, J. Auxiliary Density Matrix Methods for Hartree–Fock Exchange Calculations. *J. Chem. Theory Comput.* **2010**, *6* (8), 2348– 2364, DOI: 10.1021/ct1002225
57. Even, J.; Pedesseau, L.; Jancu, J.-M.; Katan, C. Importance of Spin–Orbit Coupling in Hybrid Organic/Inorganic Perovskites for Photovoltaic Applications. *J. Phys. Chem. Lett.* **2013**, *4* (17), 2999– 3005, DOI: 10.1021/jz401532q
58. Umari, P.; Mosconi, E.; De Angelis, F. Relativistic GW Calculations on $\text{CH}_3\text{NH}_3\text{PbI}_3$ and $\text{CH}_3\text{NH}_3\text{SnI}_3$ Perovskites for Solar Cell Applications. *Sci. Rep.* **2015**, *4*, 4467, DOI: 10.1038/srep04467
59. Hao, F.; Stoumpos, C. C.; Chang, R. P. H.; Kanatzidis, M. G. Anomalous Band Gap Behavior in Mixed Sn and Pb Perovskites Enables Broadening of Absorption Spectrum in Solar Cells. *J. Am. Chem. Soc.* **2014**, *136* (22), 8094– 8099, DOI: 10.1021/ja5033259
60. Halgren, T. A.; Lipscomb, W. N. The Synchronous-Transit Method for Determining Reaction Pathways and Locating Molecular Transition States. *Chem. Phys. Lett.* **1977**, *49* (2), 225– 232, DOI: 10.1016/0009-2614(77)80574-5
61. Quarti, C.; Mosconi, E.; De Angelis, F. Interplay of Orientational Order and Electronic Structure in Methylammonium Lead Iodide: Implications for Solar Cell Operation. *Chem. Mater.* **2014**, *26* (22), 6557– 6569, DOI: 10.1021/cm5032046
62. Liechtenstein, A. I.; Anisimov, V. I.; Zaanen, J. Density-Functional Theory and Strong Interactions: Orbital Ordering in Mott-Hubbard Insulators. *Phys. Rev. B: Condens. Matter Mater. Phys.* **1995**, *52* (8), R5467– R5470, DOI: 10.1103/PhysRevB.52.R5467
63. Dudarev, S. L.; Botton, G. A.; Savrasov, S. Y.; Humphreys, C. J.; Sutton, A. P. Electron-Energy-Loss Spectra and the Structural Stability of Nickel Oxide: An LSDA+U study. *Phys. Rev. B: Condens. Matter Mater. Phys.* **1998**, *57* (3), 1505– 1509, DOI: 10.1103/PhysRevB.57.1505
64. Du, M.-H. Density Functional Calculations of Native Defects in $\text{CH}_3\text{NH}_3\text{PbI}_3$: Effects of Spin–Orbit Coupling and Self-Interaction Error. *J. Phys. Chem. Lett.* **2015**, *6* (8), 1461– 1466, DOI: 10.1021/acs.jpclett.5b00199
65. Meggiolaro, D.; Mosconi, E.; De Angelis, F. Formation of Surface Defects Dominates Ion Migration in Lead-Halide Perovskites. *ACS Energy Lett.* **2019**, *4* (3), 779– 785, DOI: 10.1021/acsenerylett.9b00247
66. Meggiolaro, D.; Mosconi, E.; Proppe, A. H.; Quintero-Bermudez, R.; Kelley, S. O.; Sargent, E. H.; De Angelis, F. Energy Level Tuning at the MAPbI_3 Perovskite/Contact Interface Using Chemical Treatment. *ACS Energy Lett.* **2019**, *4* (9), 2181– 2184, DOI: 10.1021/acsenerylett.9b01584
67. Quarti, C.; De Angelis, F.; Beljonne, D. Influence of Surface Termination on the Energy Level Alignment at the $\text{CH}_3\text{NH}_3\text{PbI}_3$ Perovskite/ C_{60} Interface. *Chem. Mater.* **2017**, *29* (3), 958– 968, DOI: 10.1021/acs.chemmater.6b03259
68. Meggiolaro, D.; Mosconi, E.; De Angelis, F. Modeling the Interaction of Molecular Iodine with MAPbI_3 : A Probe of Lead-Halide Perovskites Defect Chemistry. *ACS Energy Lett.* **2018**, *3* (2), 447– 451, DOI: 10.1021/acsenerylett.7b01244
69. Kim, G. Y.; Senocrate, A.; Yang, T.-Y.; Gregori, G.; Grätzel, M.; Maier, J. Large Tunable Photoeffect on Ion Conduction in Halide Perovskites and Implications for Photodecomposition. *Nat. Mater.* **2018**, *17* (5), 445– 449, DOI: 10.1038/s41563-018-0038-0

70. Samu, G. F.; Balog, Á.; De Angelis, F.; Meggiolaro, D.; Kamat, P. V.; Janáky, C. Electrochemical Hole Injection Selectively Expels Iodide from Mixed Halide Perovskite Films. *J. Am. Chem. Soc.* **2019**, *141* (27), 10812– 10820, DOI: 10.1021/jacs.9b04568
71. Sadoughi, G.; Starr, D. E.; Handick, E.; Stranks, S. D.; Gorgoi, M.; Wilks, R. G.; Bär, M.; Snaith, H. J. Observation and Mediation of the Presence of Metallic Lead in Organic–Inorganic Perovskite Films. *ACS Appl. Mater. Interfaces* **2015**, *7* (24), 13440– 13444, DOI: 10.1021/acsami.5b02237